

Instantaneous phase synchronization of two decoupled quantum limit-cycle oscillators induced by conditional photon detection

Yuzuru Kato^{1,*} and Hiroya Nakao¹

¹*Department of Systems and Control Engineering,
Tokyo Institute of Technology, Tokyo 152-8552, Japan*

(Dated: December 22, 2024)

We show that conditional photon detection induces instantaneous phase synchronization between two decoupled quantum limit-cycle oscillators. We consider two quantum van der Pol oscillators without mutual coupling, each with an additional linearly coupled bath, and perform continuous measurement of photon counting on the output fields of the two baths interacting through a beam splitter. It is observed that in-phase or anti-phase coherence of the two decoupled oscillators instantaneously increases after the photon detection and then decreases gradually in the weak quantum regime or quickly in the strong quantum regime until the next photon detection occurs. In the strong quantum regime, quantum entanglement also increases after the photon detection and quickly disappears. We derive the analytical upper bounds for the increases in the quantum entanglement and phase coherence by the conditional photon detection in the quantum limit.

arXiv:2009.08286v1 [nlin.AO] 17 Sep 2020

* Corresponding author: kato.y.bg@m.titech.ac.jp

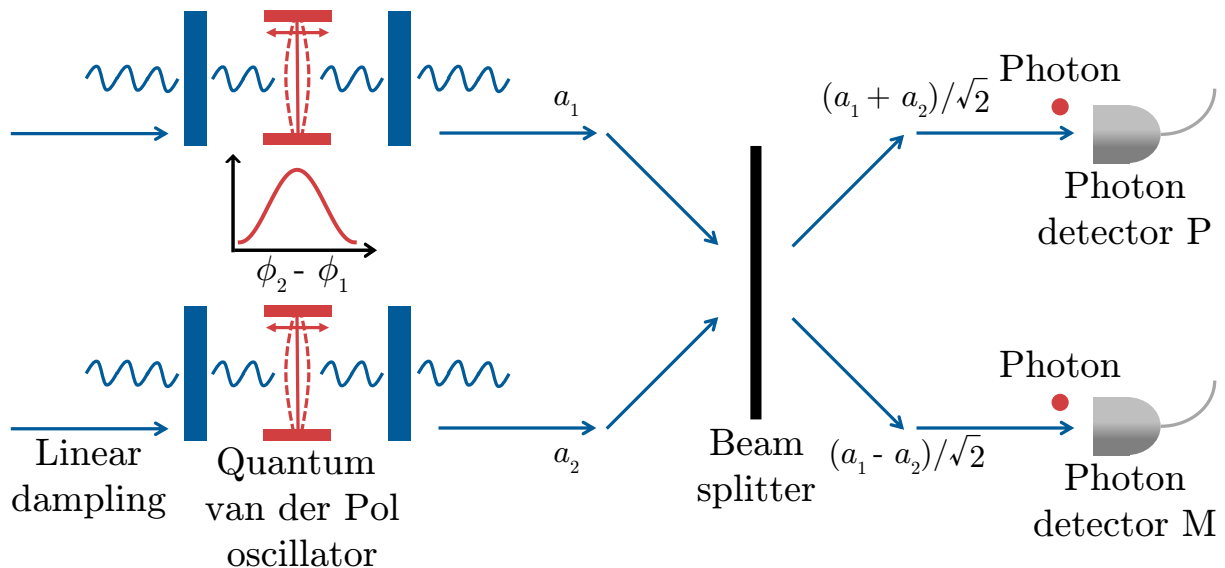


FIG. 1. Instantaneous phase synchronization of two decoupled quantum vdP oscillators induced by conditional photon detection. Either in-phase or anti-phase coherence is induced after photon detection at detector P or M, respectively.

I. INTRODUCTION

Synchronization phenomena, first reported by Huygens in the 17th century, are widely observed in various areas of science and engineering, including laser oscillations, mechanical vibrations, oscillatory chemical reactions, and biological rhythms [1–6]. While synchronization of *coupled* or *periodically driven* nonlinear oscillators has been extensively investigated [1–3, 7], oscillators that *do not involve any interactions or periodic forcing* can also exhibit synchronous behaviors when driven by common random forcing, such as consistency or reproducibility of laser oscillations and spiking neocortical neurons receiving identical sequences of random signals [8, 9]. The common-noise-induced synchronization has been theoretically investigated for decoupled limit-cycle oscillators subjected, e.g., to common random impulses [10–12] and Gaussian white noise [13–15].

Recent developments in nanotechnology have inspired theoretical investigations of quantum synchronization [16–39], and the first experimental demonstration of quantum phase synchronization in spin-1 atoms [40] and on the IBM Q system [41] has been reported very recently. Many studies have analyzed coupled quantum nonlinear dissipative oscillators, for example, synchronization of quantum van der Pol (vdP) oscillators [16–18], synchronization of ensembles of atoms [19], synchronization of triplet spins [20], measures for quantum synchronization of two oscillators [21–23], and synchronization blockade [24, 25]. The effects of quantum measurement backaction on quantum nonlinear dissipative oscillators have also been investigated as a unique feature of quantum systems, including improvement in the accuracy of Ramsey spectroscopy through measurement of synchronized atoms [26], measurement-induced transition between in-phase and anti-phase synchronized states [27], unraveling of nonclassicality in optomechanical oscillators [42], characterization of synchronization using quantum trajectories [28], and enhancement of synchronization by quantum measurement and feedback control [29].

In this study, inspired by the common-noise-induced synchronization of decoupled classical oscillators, we consider phase synchronization of two decoupled quantum oscillators induced by common backaction of quantum measurement. We consider two quantum van der Pol oscillators without mutual coupling, each with an additional linearly coupled bath, and perform continuous measurement of photon counting on the output fields of the two baths interacting through a beam splitter. It is demonstrated that the quantum measurement backaction of conditional photon detection common to both oscillators induces instantaneous phase synchronization of the oscillators.

II. MODEL

A schematic of the physical setup is depicted in Fig. 1. The stochastic master equation (SME) of the system can be expressed as

$$\begin{aligned} d\rho &= \mathcal{L}_0\rho dt + \mathcal{G}[L_+] \rho \left(dN_+ - \gamma_3 \text{Tr}[L_+^\dagger L_+ \rho] dt \right) + \mathcal{G}[L_-] \rho \left(dN_- - \gamma_3 \text{Tr}[L_-^\dagger L_- \rho] dt \right), \\ \mathcal{L}_0\rho &= \sum_{j=1,2} \left(-i \left[\omega a_j^\dagger a_j, \rho \right] + \gamma_1 \mathcal{D}[a_j^\dagger] \rho + \gamma_2 \mathcal{D}[a_j^2] \rho + \gamma_3 \mathcal{D}[a_j] \rho \right), \\ L_\pm &= \frac{1}{\sqrt{2}}(a_1 \pm a_2), \quad \mathcal{D}[L] \rho = L \rho L^\dagger - \frac{1}{2} (\rho L^\dagger L + L^\dagger L \rho), \quad \mathcal{G}[L] \rho = \frac{L \rho L^\dagger}{\text{Tr}[L \rho L^\dagger]} - \rho, \end{aligned} \quad (1)$$

where the natural frequency ω and the decay rates γ_1 , γ_2 , and γ_3 for negative damping, nonlinear damping, and linear damping, respectively, are assumed identical for both oscillators, N_\pm are two independent Poisson processes whose increments are given by $dN_\pm = 1$ with probability $\gamma_3 \text{Tr}[L_\pm^\dagger L_\pm] dt$ and $dN_\pm = 0$ with probability $1 - \gamma_3 \text{Tr}[L_\pm^\dagger L_\pm] dt$ in each interval dt , where $dN_+ = 1$ and $dN_- = 1$ represent the photon detection at detectors P and M in Fig. 1, respectively, and the reduced Planck constant is set to $\hbar = 1$. The SLH framework [43, 44] has been used to describe the cascade and concatenate connections of the quantum system components in the derivation of the SME (1) [see Appendix A for the derivation of the SME (1)].

III. WEAK QUANTUM REGIME

First, we numerically analyze the quantum SME (1) in the weak quantum regime. To characterize the degree of phase coherence between the two quantum vdP oscillators, we use the absolute value of the normalized correlator [27]

$$S_{12} = |S_{12}| e^{i\theta_{12}} = \frac{\text{Tr}[a_1^\dagger a_2 \rho]}{\sqrt{\text{Tr}[a_1^\dagger a_1 \rho] \text{Tr}[a_2^\dagger a_2 \rho]}} \quad (2)$$

as the order parameter, which is a quantum analog of the order parameter for two classical noisy oscillators [3]. The modulus $|S_{12}|$ takes values in $0 \leq |S_{12}| \leq 1$; $|S_{12}| = 1$ when the two oscillators are perfectly phase-synchronized and $|S_{12}| = 0$ when they are perfectly phase-incoherent. We also use the argument θ_{12} to characterize the averaged phase difference of the two oscillators in order to distinguish in-phase and anti-phase coherence. We use the negativity $\mathcal{N} = (\|\rho^{\Gamma_1}\|_1 - 1)/2$ to quantify the quantum entanglement of the two oscillators, where ρ^{Γ_1} represents the partial transpose of the system with respect to the subsystem representing the first oscillator and $\|X\|_1 = \text{Tr}|X| = \text{Tr}\sqrt{X^\dagger X}$ [45, 46]. When the two oscillators are entangled with one other, \mathcal{N} takes a nonzero value. We also observe the purity $P = \text{Tr}[\rho^2]$.

Figures 2(a), 2(b), 2(c), and 2(d) plot the time evolution of $|S_{12}|$, θ_{12} , \mathcal{N} , and P in the weak quantum regime, respectively, calculated for a single trajectory of the quantum SME (1). As shown in Fig. 2(a), $|S_{12}|$ instantaneously increases after the detection of a photon either at P or M, indicating that phase coherence of the two decoupled oscillators is induced by the conditional photon detection. After the photon detection, $|S_{12}|$ gradually decreases because the two oscillators converge to the desynchronized steady state of the SME (1) in the absence of photon detection, i.e., $dN_\pm = 0$.

In this regime, the nonlinear damping is not strong and the relaxation to the desynchronized state is relatively slow. Therefore, the subsequent photon detection typically occurs before the convergence to the desynchronized state and $|S_{12}|$ remains always positive. Figure 2(b) shows that θ_{12} takes either $\theta_{12} = 0$ or $\theta_{12} = \pi$. This indicates that the two oscillators immediately attain in-phase coherence after the photon detection at P or anti-phase coherence after the photon detection at M. The negativity and purity are shown in Fig. 3(c) and 3(d), respectively, where the negativity is always zero and the purity takes small values between 0.03 and 0.05, indicating that the system is separable and mixed.

The phase coherence of the two oscillators can also be captured by using the Hushimi Q distribution of the phase difference $\theta = \phi_2 - \phi_1$ [47] between the two oscillators, $Q(\theta)$, calculated by introducing the two-mode Q distribution [48] $Q(\alpha_1, \alpha_1^*, \alpha_2, \alpha_2^*) = \frac{1}{\pi^2} \langle \alpha_1, \alpha_2 | \rho | \alpha_1, \alpha_2 \rangle$ with $R_j e^{i\phi_j} = \alpha_j$ ($j = 1, 2$) and integrating over R_1 , R_2 , and $\phi_1 + \phi_2$. Figures 2(e) and 2(f) show $Q(\theta)$ of the system states immediately after the first photon detection at the detectors P and M, respectively. The peak of $Q(\theta)$ occurs at $\theta = 0$ in Fig. 2(e) and at $\theta = \pi$ in Fig. 2(f), clearly indicating that in-phase and anti-phase coherence of the two oscillators are induced by the conditional photon detection.

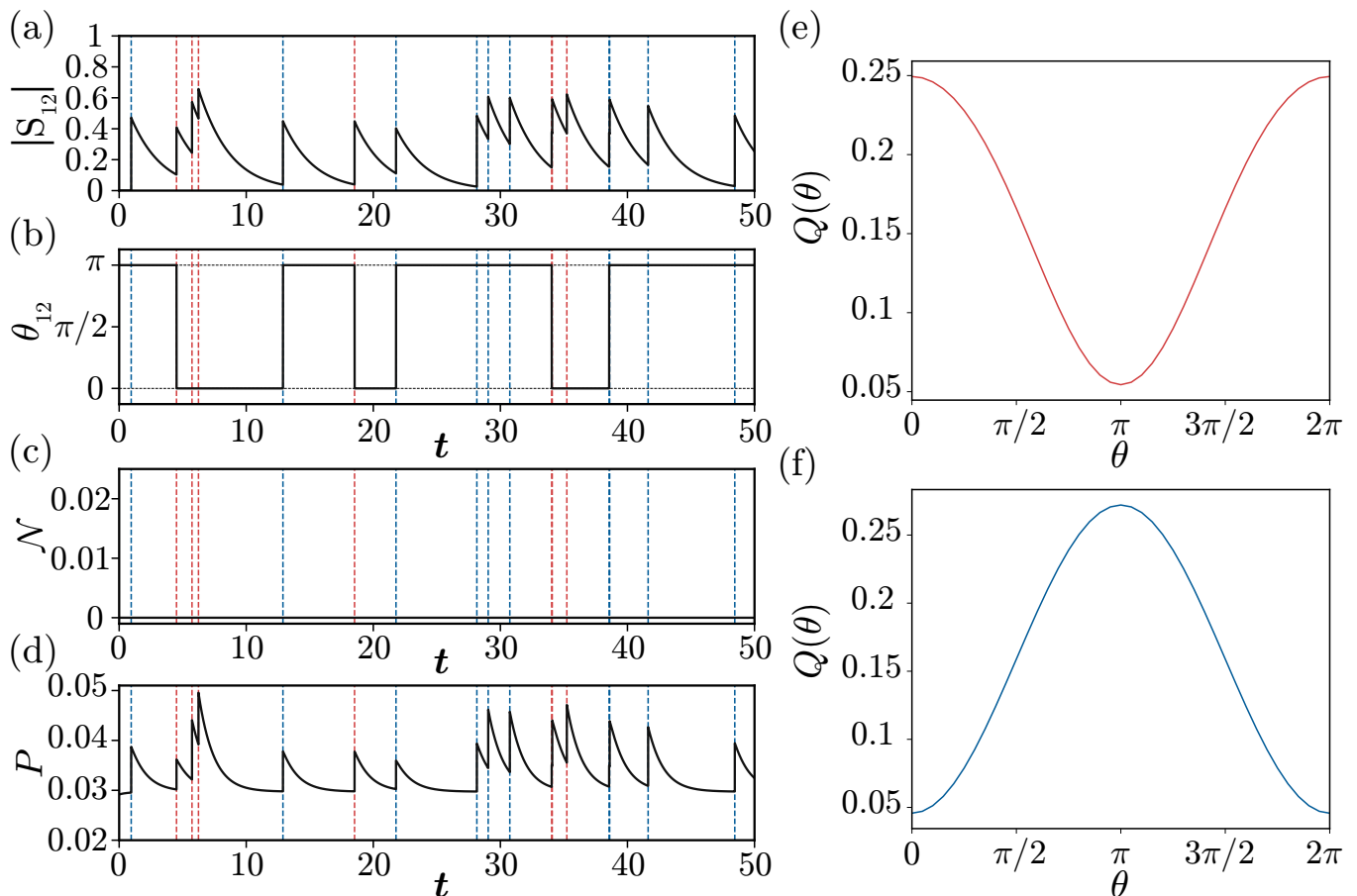


FIG. 2. Results in the weak quantum regime. The parameters are $(\omega, \gamma_2, \gamma_3)/\gamma_1 = (0.1, 0.25, 0.1)$ with $\gamma_1 = 1$. (a-d): Time evolution of (a) absolute value of the normalized correlator $|S_{12}|$, (b) average phase value θ_{12} , (c) negativity \mathcal{N} , and (d) purity P . (e,f): Q distributions $Q(\theta)$ immediately after the first photon detection at (e) P ($t = 4.51$) and (f) M ($t = 0.95$). The photon detection at detectors P and M is indicated by the red- and blue-dashed lines in (a-d), respectively.

IV. STRONG QUANTUM REGIME

We next analyze the quantum SME (1) in a stronger quantum regime. Figures 3(a), 3(b), 3(c), and 3(d) show the evolution of $|S_{12}|$, θ_{12} , \mathcal{N} , and P , respectively. As shown in Fig. 3(a), $|S_{12}|$ takes large values close to 1 immediately after the photon detection, indicating that instantaneous phase coherence also arises in this case. In this regime, the nonlinear damping is strong and the system quickly converges to the desynchronized steady state of the SME (1) when the detection does not occur, i.e., $dN_{\pm} = 0$. Therefore, the phase coherence quickly disappears and $|S_{12}|$ remains zero until the next photon detection occurs.

Similar to Fig. 2(b), Fig. 3(b) shows that θ_{12} takes either $\theta_{12} = 0$ or $\theta_{12} = \pi$. Thus, the two oscillators become in-phase coherent after the photon detection at P and anti-phase coherent after the photon detection at M. Remarkably, Figs. 3(c) and 3(d) show that non-zero negativity and purity with values between 0.5 and 0.6 are attained instantaneously after the photon detection, indicating that mixed entangled states are obtained in this case. However, the quantum entanglement quickly disappears as shown in the inset in Fig. 3(c). Figures 3(e) and 3(f) show the Q distributions $Q(\theta)$ of the system states immediately after the first photon detection at the detectors P and M, respectively. The Q distributions are peaked at $\theta = 0$ and $\theta = \pi$, clearly indicating that in-phase and anti-phase coherence of the two oscillators are induced also in this case.

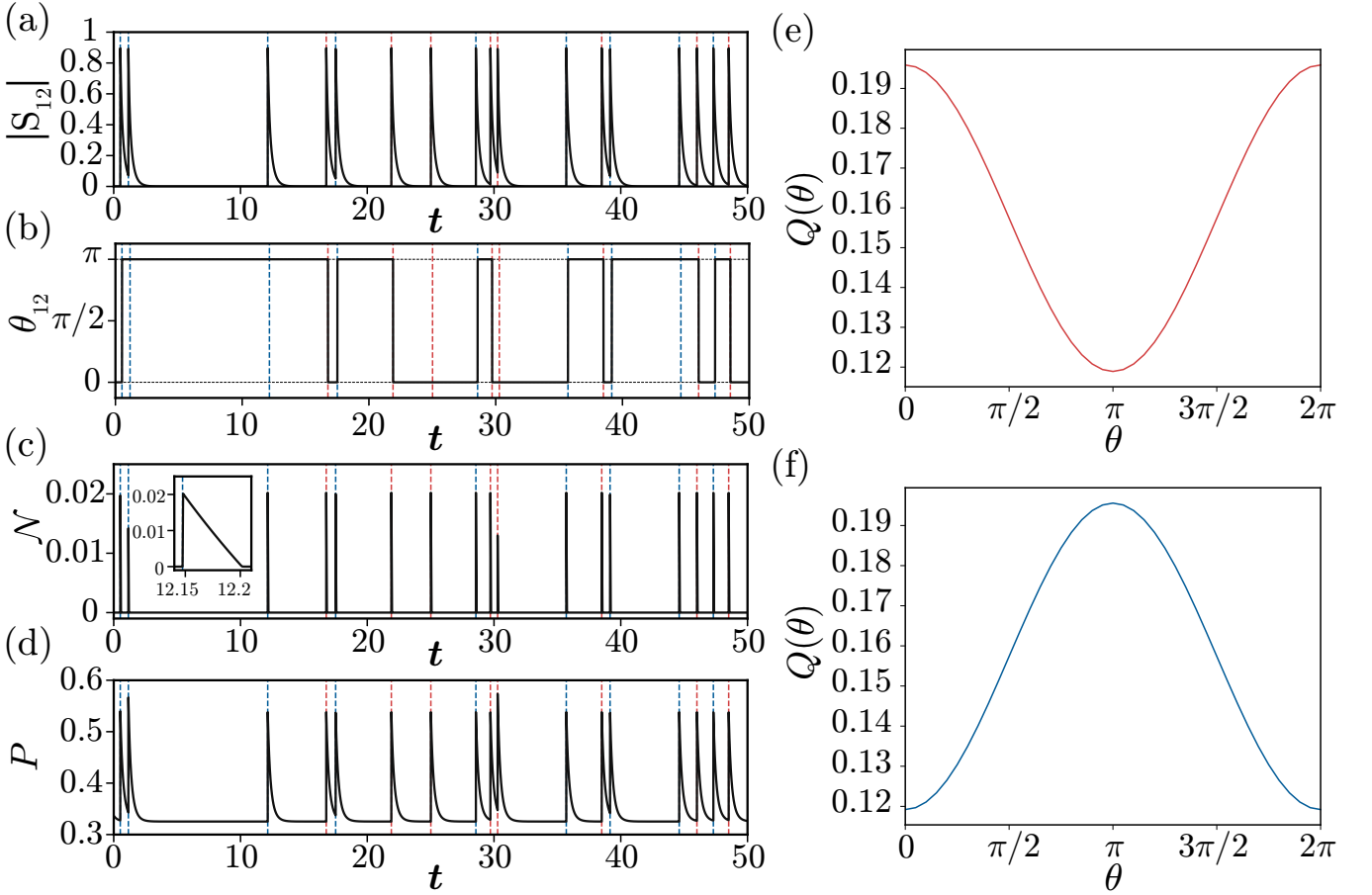


FIG. 3. Results in the strong quantum regime. The parameters are $(\omega, \gamma_2, \gamma_3)/\gamma_1 = (0.5, 50, 0.5)$ with $\gamma_1 = 1$. (a-d): Time evolution of (a) absolute value of the normalized correlator $|S_{12}|$, (b) averaged phase value θ_{12} , (c) negativity \mathcal{N} , and (d) purity P . (e, f): Q distributions $Q(\theta)$ immediately after the first photon detection at (e) P ($t = 16.8$) and (f) M ($t = 0.52$). The photon detection at detectors P and M is indicated by the red- and blue-dashed lines in (a-d), respectively.

V. QUANTUM LIMIT

From the previous numerical results, it is expected that the maximum quantum entanglement is attained in the quantum limit, i.e., $\gamma_2 \rightarrow \infty$. In this limit, we can map the quantum vdP oscillator to an analytically tractable two-level system with basis states $|0\rangle$ and $|1\rangle$ [17], and transform the SME (1) to

$$\begin{aligned}
 d\rho &= \mathcal{L}_0^q \rho dt + \mathcal{G}[L_+^q] \rho (dN_+ - \gamma_3 \text{Tr}[L_+^{q\dagger} L_+^q \rho] dt) + \mathcal{G}[L_-^q] \rho (dN_- - \gamma_3 \text{Tr}[L_-^{q\dagger} L_-^q \rho] dt), \\
 \mathcal{L}_0^q \rho &= \sum_{j=1,2} (-i [\omega \sigma_j^+ \sigma_j^-, \rho] + \gamma_1 \mathcal{D}[\sigma_j^+] \rho + (2\gamma_1 + \gamma_3) \mathcal{D}[\sigma_j^-] \rho), \quad L_\pm^q = \frac{1}{\sqrt{2}} (\sigma_1^- \pm \sigma_2^-),
 \end{aligned} \tag{3}$$

with $\sigma_j^- = |0\rangle\langle 1|_j$ and $\sigma_j^+ = |1\rangle\langle 0|_j$ representing the lowering and raising operators of the j th system ($j = 1, 2$), respectively, because the transition $|1\rangle \xrightarrow{2\gamma_1} |2\rangle \xrightarrow{2\gamma_3} |0\rangle$ can be regarded as $|1\rangle \xrightarrow{2\gamma_1} |0\rangle$ when $\gamma_2 \rightarrow \infty$.

The steady state of Eq. (3) without detection, i.e., $dN_\pm = 0$, can be analytically obtained, which is given by a

diagonal matrix $\rho^{pre} = \text{diag}(\rho_0^{pre}, \rho_1^{pre}, \rho_1^{pre}, \rho_2^{pre})$ with

$$\begin{aligned}\rho_0^{pre} &= \frac{(k-3)\sqrt{k^2+2k+9} + k^2 - 2k + 9}{2k^2}, \\ \rho_1^{pre} &= \frac{3\sqrt{k^2+2k+9} - k - 9}{2k^2}, \\ \rho_2^{pre} &= \frac{-(k+3)\sqrt{k^2+2k+9} + k^2 + 4k + 9}{2k^2}.\end{aligned}\quad (4)$$

Note that only a single parameter $k = \gamma_3/\gamma_1$ specifies the elements of the matrix, where we assume $k > 0$, namely, the photon detection occurs with a non-zero probability.

The states $\rho_{\pm}^{pos} = L_{\pm}^q \rho^{pre} L_{\pm}^{q\dagger} / \text{Tr}[L_{\pm}^q \rho^{pre} L_{\pm}^{q\dagger}]$ immediately after the photon detection occurs at the detector P (ρ_+^{pos}) and M (ρ_-^{pos}) can be represented by a density matrix

$$\rho_{\pm}^{pos} = \rho_0^{pos} |00\rangle\langle 00| + \rho_1^{pos} \left(\frac{|01\rangle \pm |10\rangle}{\sqrt{2}} \right) \left(\frac{\langle 01| \pm \langle 10|}{\sqrt{2}} \right) \quad (5)$$

with

$$\begin{aligned}\rho_0^{pos} &= \frac{-3\sqrt{k^2+2k+9} + k + 9}{k(\sqrt{k^2+2k+9} - k - 3)}, \\ \rho_1^{pos} &= \frac{(k+3)\sqrt{k^2+2k+9} - k^2 - 4k - 9}{k(\sqrt{k^2+2k+9} - k - 3)}.\end{aligned}\quad (6)$$

Using this result, we can explicitly calculate the normalized correlator S_{12} and the Q distribution of the phase difference between the two oscillators.

In this case, the correlator S_{12} of the states ρ_{\pm}^{pos} immediately after the photon detection always takes $S_{12} = \pm 1$ irrespective of the value of k (and then quickly decays). The Q distribution for ρ_{\pm}^{pos} can also be calculated as (similar calculation for the Wigner distribution of the phase difference has been performed in [17])

$$Q(\theta)[\rho_{\pm}^{pos}] = \frac{1}{2\pi} \pm \frac{\rho_1^{pos} \cos \theta}{8}. \quad (7)$$

These results qualitatively agree with the corresponding results in the strong quantum regime in Fig. 3. It is notable that the dependence of the phase coherence on k can be captured by the peak height of $Q(\theta)$ but not by the normalized correlator S_{12} in the quantum limit. Indeed, the element $\rho_0^{pos}|00\rangle\langle 00|$ in Eq. (5) affects $Q(\theta)$ (through $\rho_1^{pos} = 1 - \rho_0^{pos}$) in Eq. (7), whereas it does not affect the value of S_{12} .

The above result indicates that the degree of phase coherence is better quantified by the peak height of $Q(\theta)$ rather than S_{12} in strong quantum regimes. This is because S_{12} is defined as a quantum analog of the order parameter for the coherence of classical noisy oscillators, which is quantitatively correct only in the semiclassical regime. This observation is also important in interpreting the results in the weak and strong quantum regimes shown in Figs. 2 and 3, where $Q(\theta)$ in the weak quantum regime (Fig. 2) are more sharply peaked than those in the strong quantum regime (Fig. 3), while $|S_{12}|$ in Fig. 2 takes smaller values than that in Fig. 3. Thus, S_{12} may not work well for comparing phase coherence between different quantum regimes.

In the quantum limit, the symmetric superpositions $|S\rangle = (|01\rangle + |10\rangle)/\sqrt{2}$ and $|A\rangle = (|01\rangle - |10\rangle)/\sqrt{2}$ can be regarded as the in-phase and anti-phase synchronized states, because the corresponding distributions $Q(\theta)[|S\rangle\langle S|] = \frac{1}{2\pi} + \frac{\cos \theta}{8}$ and $Q(\theta)[|A\rangle\langle A|] = \frac{1}{2\pi} - \frac{\cos \theta}{8}$ are peaked at $\theta = 0$ and $\theta = \pi$, respectively. As $|A\rangle$ and $|S\rangle$ are dark states with respect to L_+^q and L_-^q , i.e., $L_+^q|A\rangle = 0$ and $L_-^q|S\rangle = 0$, the photon detection at the detector P annihilates the anti-phase-synchronized state $|A\rangle$ and creates the in-phase synchronized state $|S\rangle$ with $S_{12} = 1$ ($\theta_{12} = 0$), while the photon detection at the detector M annihilates $|S\rangle$ and creates $|A\rangle$ with $S_{12} = -1$ ($\theta_{12} = \pi$).

Figures 4(a), 4(b), and 4(c) show the dependence of the elements ρ^{pre} and ρ^{pos} and $Q(\theta)[\rho_+^{pos}]$ on k , respectively (we only plot $Q(\theta)[\rho_+^{pos}]$ because $Q(\theta)[\rho_-^{pos}] = Q(\theta + \pi)[\rho_+^{pos}]$). As shown in Fig. 4(a), ρ_1^{pre} and ρ_2^{pre} take larger values when k is smaller. When $k \rightarrow 0$, ρ_1^{pre} and ρ_2^{pre} approach the supremum values, $\rho_1^{pre} \rightarrow \frac{2}{9}$ and $\rho_2^{pre} \rightarrow \frac{1}{9}$ ($\rho_0^{pre} \rightarrow \frac{4}{9}$), corresponding to the completely incoherent steady state of the two decoupled quantum vdP oscillators in the quantum limit, i.e., $\rho^{pre} \rightarrow (\frac{2}{3}|0\rangle\langle 0| + \frac{1}{3}|1\rangle\langle 1|) \otimes (\frac{2}{3}|0\rangle\langle 0| + \frac{1}{3}|1\rangle\langle 1|)$, where $Q(\theta)$ is uniform [16, 17]. Therefore, ρ_1^{pos} approaches the supremum value, $\rho_1^{pos} \rightarrow \frac{1}{3}$ ($\rho_0^{pos} \rightarrow \frac{2}{3}$), as shown in Fig. 4(b), and $Q(\theta)[\rho_+^{pos}]$ exhibits the maximum peak as shown in Fig. 4(c), indicating that the maximum phase coherence is obtained. In the opposite limit, $k \rightarrow \infty$, ρ^{pre} converges to the two-mode vacuum state $\rho^{pre} \rightarrow |00\rangle\langle 00|$, i.e., $\rho_1^{pre}, \rho_2^{pre} \rightarrow 0$ ($\rho_0^{pre} \rightarrow 1$), resulting in $\rho_1^{pos} \rightarrow 0$ ($\rho_0^{pos} \rightarrow 1$) and the uniform distribution $Q(\theta)[\rho_+^{pos}] \rightarrow \frac{\pi}{2}$.

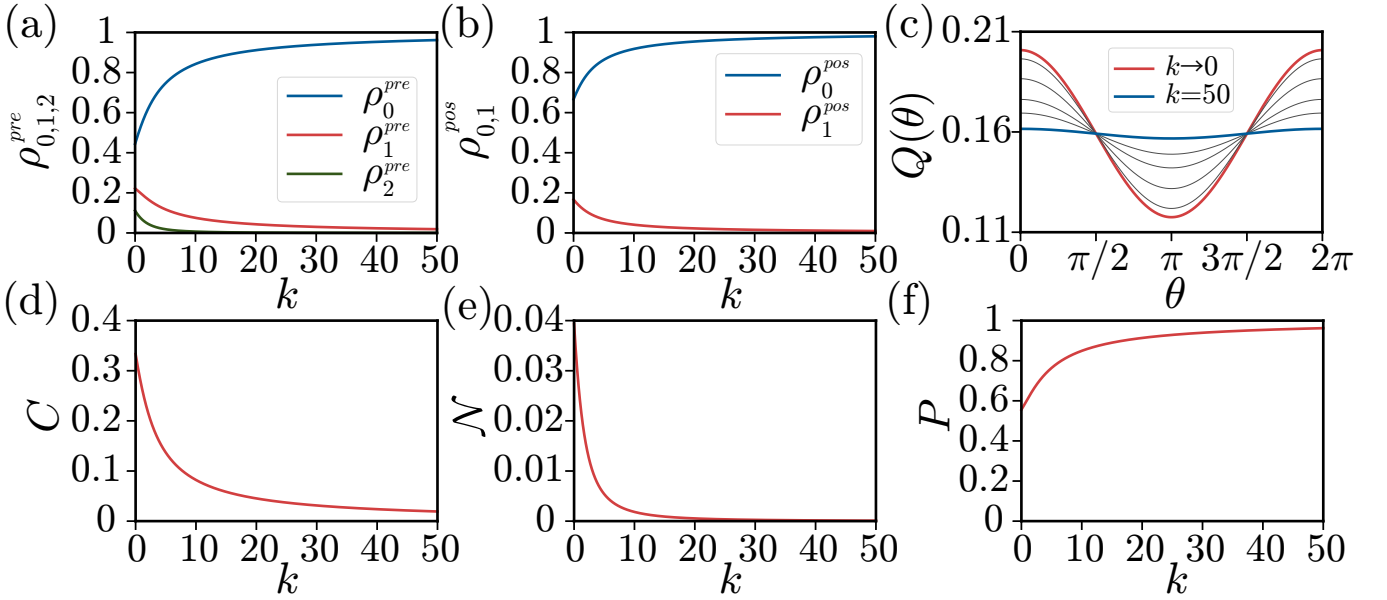


FIG. 4. Dependence of the results on the parameter $k = \gamma_3/\gamma_1$ of the two-level system in the quantum limit $\gamma_2 \rightarrow \infty$. (a) Elements of ρ^{pre} . (b) Elements of ρ^{pos} . (c) $Q(\theta)[\rho_+^{pos}]$ distributions of the phase difference of two oscillators for $k \rightarrow 0$ (red line), $k = 0.5, 2, 5, 10$ (gray lines from the red line to the blue line), and $k = 50$ (blue line) are shown. (d) Concurrence. (e) Negativity. (f) Purity.

In addition to the negativity \mathcal{N} and purity P , the quantum entanglement of the density matrix ρ_{pos} in Eq. (5) can also be quantified using the concurrence [49], $C = \max(0, \lambda_1 - \lambda_2 - \lambda_3 - \lambda_4)$, where $\lambda_1, \lambda_2, \lambda_3$, and λ_4 are the square roots of the eigenvalues of $\rho\tilde{\rho}$ with $\tilde{\rho} = (\sigma_y \otimes \sigma_y)\rho^*(\sigma_y \otimes \sigma_y)$ in decreasing order. The concurrence C takes a non-zero value when the two oscillators are entangled with each other ($C \in [0, 1]$ by definition).

Figures 4(d), 4(e), and 4(f) show the dependence of C , \mathcal{N} and P on k for ρ_{\pm}^{pos} , respectively. Note that C , \mathcal{N} , and P take the same values for both ρ_+ and ρ_- . In the limit $k \rightarrow 0$, C , \mathcal{N} , and P approach the upper bounds as $C \rightarrow \frac{1}{3}$, $\mathcal{N} \rightarrow \frac{\sqrt{5}-2}{6}$, and $P \rightarrow \frac{5}{9}$. In the opposite limit $k \rightarrow \infty$, these values converge as $C \rightarrow 0$, $\mathcal{N} \rightarrow 0$, and $P \rightarrow 1$, which corresponds to those quantities for the two-mode vacuum states.

Photon detection occurs less frequently when k is smaller, because the probability of the photon detection in the interval dt at detectors P or M is given by $k \text{Tr} [L_{\pm}^{\dagger} L_{\pm}] \gamma_1 dt$. Therefore, on average, infinitely-long observation time is required before the photon detection to approach the upper bounds for the degree of phase coherence and quantum entanglement in the limit $k \rightarrow 0$.

VI. CONCLUSION

We have analyzed two decoupled quantum van der Pol oscillators and demonstrated that quantum measurement backaction of conditional photon detection induces instantaneous phase synchronization of the oscillators. In-phase or anti-phase coherence between the oscillators has been observed instantaneously after the photon detection, which decays gradually in the weak quantum regime or quickly in the strong quantum regime until the next photon detection. In the strong quantum regime, short-time increase in the quantum entanglement has also been observed. In the quantum limit, we analytically obtained the upper bounds for the increases in the quantum entanglement and phase coherence.

Recently, physical implementations of the quantum vdP oscillator with ion trap systems [16, 17] and optomechanical systems [18, 31] have been discussed. The additional linearly coupled bath and photon detectors can also be introduced [48, 50]. The physical setup considered in the present study does not require explicit mutual coupling between the oscillators. Therefore, it can, in principle, be implemented by using existing experimental methods and provide a method for generating phase-coherent states of quantum limit-cycle oscillators.

Acknowledgments.- The numerical simulations are performed by using the QuTiP numerical toolbox [51]. We acknowledge JSPS KAKENHI JP17H03279, JP18H03287, JPJSBP120202201, JP20J13778, and JST CREST JP-

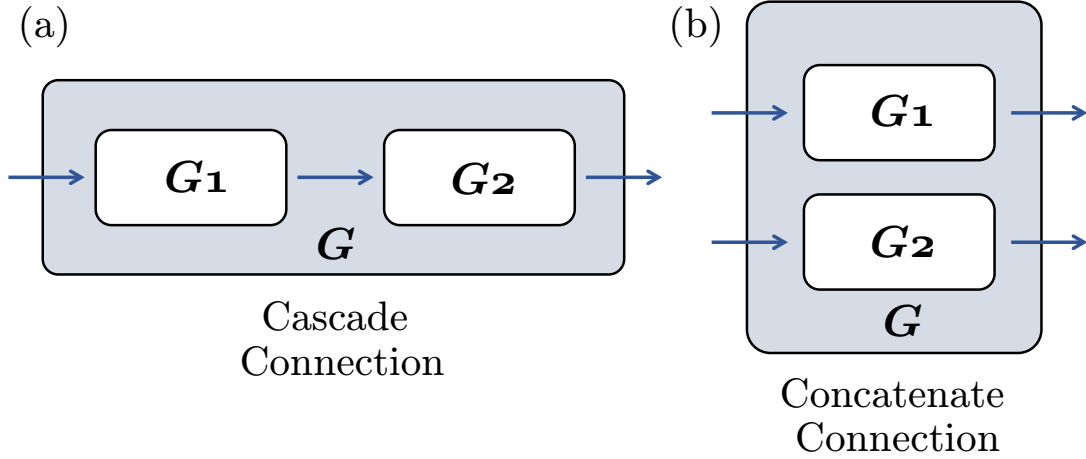


FIG. 5. (a) Cascade and concatenate connection of the two system components G_1 and G_2 .

MJCR1913 for financial support.

Appendix A: SLH framework

In this Appendix, we derive the SME (1) using the SLH framework to describe cascade and concatenate connections of the quantum system components [43, 44]. In this framework, the parameters in the time evolution of a quantum system ρ are specified by $\mathbf{G} = (\mathbf{S}, \mathbf{L}, H)$, with

$$\mathbf{S} = \begin{pmatrix} S_{11} & \cdots & S_{1n} \\ \vdots & & \vdots \\ S_{n1} & \cdots & S_{nn} \end{pmatrix}, \quad \mathbf{L} = \begin{pmatrix} L_1 \\ \vdots \\ L_n \end{pmatrix}, \quad (\text{A1})$$

where \mathbf{S} is the scattering matrix with operator entries satisfying $\mathbf{S}^\dagger \mathbf{S} = \mathbf{S} \mathbf{S}^\dagger = \mathbf{I}^n$, \mathbf{L} is a coupling vector with operator entries, and H is a self-adjoint operator referred to as the system Hamiltonian. We denote by \mathbf{I}^n an identity matrix with n dimensions.

With these parameters, the time evolution of the system obeys the master equation

$$\frac{d\rho}{dt} = -i[H, \rho] + \sum_{i=1}^n \mathcal{D}[L_i]\rho, \quad (\text{A2})$$

where \mathbf{S} is involved in the calculation of the cascade and concatenation products and has an important role in determining the forms of H and \mathbf{L} of the whole network system consisting of the system components. This specification of parameters is based on Hudson-Parthasarathy's work [52].

The cascade product (Fig. 5(a)) of $\mathbf{G}_1 = (\mathbf{S}_1, \mathbf{L}_1, H_1)$ and $\mathbf{G}_2 = (\mathbf{S}_2, \mathbf{L}_2, H_2)$ is given by

$$\mathbf{G}_1 \triangleleft \mathbf{G}_2 = \left(\mathbf{S}_2 \mathbf{S}_1, \mathbf{L}_2 + \mathbf{S}_2 \mathbf{L}_1, H_1 + H_2 + \frac{1}{2i} \left(\mathbf{L}_2^\dagger \mathbf{S}_2 \mathbf{L}_1 - \mathbf{L}_1^\dagger \mathbf{S}_2^\dagger \mathbf{L}_2 \right) \right), \quad (\text{A3})$$

and the concatenation product (See Fig. 5(b)) of \mathbf{G}_1 and \mathbf{G}_2 is given by

$$\mathbf{G}_1 \boxplus \mathbf{G}_2 = \left(\begin{pmatrix} \mathbf{S}_1 & 0 \\ 0 & \mathbf{S}_2 \end{pmatrix}, \begin{pmatrix} \mathbf{L}_1 \\ \mathbf{L}_2 \end{pmatrix}, H_1 + H_2 \right). \quad (\text{A4})$$

Our aim is to derive the SME (1) of the physical setup depicted in Fig. 1 [43, 44]. To this end, we denote \mathbf{G}_j^{QVDP} as the parameters of the j th quantum vdP oscillator with an additional linearly coupled bath

$$\mathbf{G}_j^{QVDP} = \left(\mathbf{I}^3, \begin{pmatrix} \sqrt{\gamma_1} a_j^\dagger \\ \sqrt{\gamma_2} a_j^2 \\ \sqrt{\gamma_3} a_j \end{pmatrix}, \omega a_j^\dagger a_j \right). \quad (\text{A5})$$

The concatenate connection of \mathbf{G}_1^{QVDP} and \mathbf{G}_2^{QVDP} is

$$\mathbf{G}_1^{QVDP} \boxplus \mathbf{G}_2^{QVDP} = \left(\mathbf{I}^6, \begin{pmatrix} \sqrt{\gamma_1} a_1^\dagger \\ \sqrt{\gamma_1} a_2^\dagger \\ \sqrt{\gamma_2} a_1^\dagger \\ \sqrt{\gamma_2} a_2^\dagger \\ \sqrt{\gamma_3} a_1 \\ \sqrt{\gamma_3} a_2 \end{pmatrix}, \sum_{j=1,2} \omega a_j^\dagger a_j \right), \quad (\text{A6})$$

where we have changed the order of the elements in \mathbf{L} for simplicity of notation.

In this study, we consider a 50:50 beam splitter. The parameters of the beam splitter \mathbf{G}^{BS} for the output fields of the two baths are

$$\mathbf{G}^{BS} = \left(\begin{pmatrix} \mathbf{I}^4 & \mathbf{O}^{42} \\ \mathbf{O}^{24} & \begin{pmatrix} \frac{1}{\sqrt{2}} & -\frac{1}{\sqrt{2}} \\ \frac{1}{\sqrt{2}} & \frac{1}{\sqrt{2}} \end{pmatrix} \end{pmatrix}, 0, 0 \right), \quad (\text{A7})$$

where we denote by \mathbf{O}^{nm} a zero matrix with the dimensions $n \times m$.

The cascading connection of the two above-mentioned components is given by

$$\mathbf{G}_1^{QVDP} \boxplus \mathbf{G}_2^{QVDP} \triangleleft \mathbf{G}^{BS} = \left(\begin{pmatrix} \mathbf{I}^4 & \mathbf{O}^{42} \\ \mathbf{O}^{24} & \begin{pmatrix} \frac{1}{\sqrt{2}} & -\frac{1}{\sqrt{2}} \\ \frac{1}{\sqrt{2}} & \frac{1}{\sqrt{2}} \end{pmatrix} \end{pmatrix}, \begin{pmatrix} \sqrt{\gamma_1} a_1^\dagger \\ \sqrt{\gamma_1} a_2^\dagger \\ \sqrt{\gamma_2} a_1^\dagger \\ \sqrt{\gamma_2} a_2^\dagger \\ \sqrt{\gamma_3} \frac{a_1 - a_2}{\sqrt{2}} \\ \sqrt{\gamma_3} \frac{a_1 + a_2}{\sqrt{2}} \end{pmatrix}, \sum_{j=1,2} \omega a_j^\dagger a_j \right). \quad (\text{A8})$$

Using transformation $\mathcal{D}[\frac{a_1+a_2}{\sqrt{2}}]\rho + \mathcal{D}[\frac{a_1-a_2}{\sqrt{2}}]\rho = \mathcal{D}[a_1]\rho + \mathcal{D}[a_2]\rho$, the quantum master equation (A2) with the parameters given in Eq. (A8) gives $d\rho = \mathcal{L}_0\rho dt$ of the SME (1). Then, using the quantum filtering theory [53, 54], SME (1) can be obtained.

-
- [1] A. T. Winfree, *The geometry of biological time* (Springer, New York, 2001).
[2] Y. Kuramoto, *Chemical oscillations, waves, and turbulence* (Springer, Berlin, 1984).
[3] A. Pikovsky, M. Rosenblum, and J. Kurths, *Synchronization: a universal concept in nonlinear sciences* (Cambridge University Press, Cambridge, 2001).
[4] H. Nakao, *Contemporary Physics* **57**, 188 (2016).
[5] G. B. Ermentrout and D. H. Terman, *Mathematical foundations of neuroscience* (Springer, New York, 2010).
[6] S. Strogatz, *Nonlinear dynamics and chaos* (Westview Press, 1994).
[7] D. G. Aronson, G. B. Ermentrout, and N. Kopell, *Physica D: Nonlinear Phenomena* **41**, 403 (1990).
[8] A. Uchida, R. McAllister, and R. Roy, *Physical review letters* **93**, 244102 (2004).
[9] Z. F. Mainen and T. J. Sejnowski, *Science* **268**, 1503 (1995).
[10] A. S. Pikovskii, *Radiophysics and Quantum Electronics* **27**, 390 (1984).
[11] H. Nakao, K.-s. Arai, K. Nagai, Y. Tsubo, and Y. Kuramoto, *Physical Review E* **72**, 026220 (2005).
[12] K. Arai and H. Nakao, *Physical Review E* **77**, 036218 (2008).
[13] J.-n. Teramae and D. Tanaka, *Physical Review Letters* **93**, 204103 (2004).
[14] D. S. Goldobin and A. S. Pikovsky, *Physica A: Statistical Mechanics and its Applications* **351**, 126 (2005).
[15] H. Nakao, K. Arai, and Y. Kawamura, *Physical Review Letters* **98**, 184101 (2007).
[16] T. E. Lee and H. Sadeghpour, *Physical Review Letters* **111**, 234101 (2013).
[17] T. E. Lee, C.-K. Chan, and S. Wang, *Physical Review E* **89**, 022913 (2014).
[18] S. Walter, A. Nunnenkamp, and C. Bruder, *Annalen der Physik* **527**, 131 (2015).
[19] M. Xu, D. A. Tieri, E. Fine, J. K. Thompson, and M. J. Holland, *Physical Review Letters* **113**, 154101 (2014).
[20] A. Roulet and C. Bruder, *Physical Review Letters* **121**, 063601 (2018).
[21] A. Mari, A. Farace, N. Didier, V. Giovannetti, and R. Fazio, *Physical Review Letters* **111**, 103605 (2013).
[22] V. Ameri, M. Eghbali-Arani, A. Mari, A. Farace, F. Kheirandish, V. Giovannetti, and R. Fazio, *Physical Review A* **91**, 012301 (2015).
[23] F. Galve, G. L. Giorgi, and R. Zambrini, in *Lectures on General Quantum Correlations and their Applications* (Springer, 2017) pp. 393–420.

- [24] N. Lörch, S. E. Nigg, A. Nunnenkamp, R. P. Tiwari, and C. Bruder, *Physical Review Letters* **118**, 243602 (2017).
- [25] S. E. Nigg, *Physical Review A* **97**, 013811 (2018).
- [26] M. Xu and M. Holland, *Physical Review Letters* **114**, 103601 (2015).
- [27] T. Weiss, A. Kronwald, and F. Marquardt, *New Journal of Physics* **18**, 013043 (2016).
- [28] N. Es' haqi Sani, G. Manzano, R. Zambrini, and R. Fazio, *Physical Review Research* **2**, 023101 (2020).
- [29] Y. Kato and H. Nakao, arXiv preprint arXiv:2009.05468 (2020).
- [30] M. Koppenhöfer and A. Roulet, *Physical Review A* **99**, 043804 (2019).
- [31] S. Walter, A. Nunnenkamp, and C. Bruder, *Physical Review Letters* **112**, 094102 (2014).
- [32] S. Sonar, M. Hajdušek, M. Mukherjee, R. Fazio, V. Vedral, S. Vinjanampathy, and L.-C. Kwek, *Physical Review Letters* **120**, 163601 (2018).
- [33] N. Lörch, E. Amitai, A. Nunnenkamp, and C. Bruder, *Physical Review Letters* **117**, 073601 (2016).
- [34] T. Weiss, S. Walter, and F. Marquardt, *Physical Review A* **95**, 041802 (2017).
- [35] A. Roulet and C. Bruder, *Physical Review Letters* **121**, 053601 (2018).
- [36] D. Witthaut, S. Wimberger, R. Burioni, and M. Timme, *Nature Communications* **8**, 14829 (2017).
- [37] Y. Kato, N. Yamamoto, and H. Nakao, *Phys. Rev. Research* **1**, 033012 (2019).
- [38] Y. Kato and H. Nakao, *Physical Review E* **101**, 012210 (2020).
- [39] Y. Kato and H. Nakao, arXiv preprint arXiv:2006.00760 (2020).
- [40] A. W. Laskar, P. Adhikary, S. Mondal, P. Katiyar, S. Vinjanampathy, and S. Ghosh, *Physical Review Letters* **125**, 013601 (2020).
- [41] M. Koppenhöfer, C. Bruder, and A. Roulet, *Physical Review Research* **2**, 023026 (2020).
- [42] M. Koppenhöfer, C. Bruder, and N. Lörch, *Physical Review A* **97**, 063812 (2018).
- [43] J. Gough and M. R. James, *IEEE Transactions on Automatic Control* **54**, 2530 (2009).
- [44] J. Combes, J. Kerckhoff, and M. Sarovar, *Advances in Physics: X* **2**, 784 (2017).
- [45] K. Życzkowski, P. Horodecki, A. Sanpera, and M. Lewenstein, *Physical Review A* **58**, 883 (1998).
- [46] G. Vidal and R. F. Werner, *Physical Review A* **65**, 032314 (2002).
- [47] K. Husimi, *Proceedings of the Physico-Mathematical Society of Japan. 3rd Series* **22**, 264 (1940).
- [48] H. J. Carmichael, *Statistical Methods in Quantum Optics 1, 2* (Springer, New York, 2007).
- [49] W. K. Wootters, *Physical Review Letters* **80**, 2245 (1998).
- [50] H. M. Wiseman and G. J. Milburn, *Quantum measurement and control* (Cambridge University Press, 2009).
- [51] J. Johansson, P. Nation, and F. Nori, *Computer Physics Communications* **183**, 1760 (2012); **184**, 1234 (2013).
- [52] R. L. Hudson and K. R. Parthasarathy, *Communications in Mathematical Physics* **93**, 301 (1984).
- [53] R. Van Handel, J. K. Stockton, and H. Mabuchi, *IEEE Transactions on Automatic Control* **50**, 768 (2005).
- [54] L. Bouten, R. Van Handel, and M. R. James, *SIAM Journal on Control and Optimization* **46**, 2199 (2007).